

New inhibitor quadrupole mutant *Pf*DHFR as antimalaria candidate: Structure-based pharmacophore, molecular docking, ADMET, molecular dynamic, and chemical quantum study

Putra Jiwamurwa Pama TJITDA^{1*}, Sree Vaneesa NAGALINGAM², Febri Odel NITBANI³, Dominus MBUNGA¹, Oemeria Sitta SUBADRA¹, Syahira Binti Mohd Abdul WAHAB^{2,4}, Maria HILARIA¹, Ibrahim ABDULLAH², Mariana Oni BETAN⁵

¹ Department of Pharmacy, Health Polytechnic of Kupang, Kupang, Indonesia

² School of Pharmacy, Management and Science University, Selangor Darul Ehsan, Malaysia

³ Department of Chemistry, Faculty of Science and Engineering, University of Nusa Cendana, Kupang, Indonesia

⁴ Centre for Drug and Herbal Development, Faculty of Pharmacy, University Kebangsaan Malaysia, Kuala Lumpur, Malaysia

⁵ Department of Nursing, Health Polytechnic of Kupang, Kupang, Indonesia

* Corresponding Author. E-mail: putratjitda@poltekkeskupang.ac.id (P.J.P.T); Tel. +62-812-373 03 590.

Received: 27 February 2024 / Revised: 31 May 2024 / Accepted: 3 June 2024

ABSTRACT: Genetic mutations in the dihydrofolate reductase-thymidylate synthase (*Pf*DHFR-TS) enzyme of the malaria parasite *Plasmodium falciparum* have been shown to reduce the effectiveness of several approved antimalarial drugs. This phenomenon has become a new challenge to the malaria control and treatment sector. As a result, the goal of this study is to identify the best compound with the potential to be an antimalarial agent by employing a good model pharmacophore generated by mutated *Pf*DHFR as a receptor. Using a computational chemistry method, a structure-based pharmacophore was utilized to analyze 165,878 compounds from the zinc database. Subsequently, these compounds were further examined by molecular docking. Furthermore, the ADMET properties, including absorption, distribution, metabolism, excretion, and toxicity, of these drug-candidates have been assessed. Furthermore, molecular dynamic simulations were employed to investigate the stability of the compound-receptor complex, while DFT investigations were utilized to examine the electronic characteristics of these compounds. Overall findings indicated that the substance C431 (ZINC257280996) may be a potent *Pf*DHFR-TS inhibitor due to its favorable binding energy of -42.26 kJ/mol, molecular dynamics simulations' indication of its stability, and its advantageous pharmacokinetic characteristics along with its non-toxic nature. The findings suggested that compound C431 could be a promising antimalarial candidate. Furthermore, this research provides guidance for improving the structure of compound C431 for future synthesis and verifies its antimalarial efficacy in vitro.

KEYWORDS: ADMET; DFT Study; Molecular Docking; Molecular Dynamic; Pharmacophore Modeling.

1. INTRODUCTION

Malaria is a life-threatening disease for humans [1]. According to the World Health Organization (WHO), in 2022, there were an estimated 608,000 deaths due to malarial infection by *Anopheles mosquitoes*. However, there was a decline in the death toll by malaria in the year 2021 [2]. This trend is expected to remain as a vision for WHO to significantly reduce the global malarial mortality rates by 2030. This disease continues to be a public health catastrophe that requires a comprehensive solution, even though various efforts have been made. Over the years, many research activities to discover malaria drugs have continued. However, several drugs that have the potential to act as antimalarials still have various weaknesses, such as low efficacy and bioavailability [3].

Numerous approaches have been conducted to find new compounds as antimalarial drug candidates. In the present scenario, computer-aided drug discovery (CADD) has become one of the most popular approaches to identifying and discovering drug candidate compounds, including antimalarials [4]. Short

How to cite this article: Tjitda PJP, Nagalingam SV, Nitbani FO, Mbunga D, Subadra OS, Wahab SBMA, Hilaria M, Abdullah I, Betan MO. New inhibitor quadrupole mutant *Pf*DHFR as antimalaria candidate: Structure-based pharmacophore, molecular docking, ADMET, molecular dynamic, and chemical quantum study. J Res Pharm. 2025; 29(2): 790-805.

identification time and minimal research costs are some of the advantages resulting from the CADD method. In addition, the drug candidates that have been discovered using the CADD method can be further modified to improve their biological activities [5]. A subsequent attempt was to utilize the molecular docking technique to discover potential molecules in a database. Compound hits were determined using a molecular docking approach based on the compounds with the lowest binding energy and their interactions with amino acid residues within the receptor binding site [6].

PfDHFR-TS, or *Plasmodium falciparum* dihydrofolate reductase-thymidylate synthase, is a crucial enzyme in antimalarial drug-candidate discovery studies. PfDHFR-TS works as a catalysator in thymidylate, purine, and methionine biosynthesis through folate formation [7]. This activity is essential to the parasite's DNA synthesis to assure their survival. Therefore, PfDHFR-TS has been a main target of antifolate-related antimalarial drug-candidate discoveries.

Pymethamine and cycloguanil are two groups of compounds that are known to stop dihydrofolate reductase (DHFR) from working. For instance, WR99210 is a natural inhibitor from the pyrimethamine derivative group, which is always in the PfDHFR complex. However, several research publications indicated that there has been a development of resistance against the pyrimethamine and cycloguanil drug groups [8–11]. Furthermore, genetic mutations in some amino acids of DHFR, such as Ala16, Ile51, Cys59, Ser108, and Ile164, have also been reported [12]. As the mutation happens to Ser108, it produces a large steric effect on the para-chlorophenyl side chain of pyrimethamine, which induces a decline in binding affinity towards the active site of DHFR [13].

Virtual screening of all compounds in a large database (Zinc Database) has the potential to produce hit compounds [14]. At present, the pharmacophore modeling approach in virtual screening is an efficient way to obtain hit compounds. Initially, each functional group that binds to the active site of the receptor is utilized as a pharmacophore feature. Afterwards, all compounds in the database are superimposed on the pharmacophore model that has been built to obtain compounds that are similar to these features. This method is known as structure-based pharmacophore [15].

This study was carried out to acquire the antifolate-antimalarial candidate compounds. The WR99210 compound was studied for its interaction on the DHFR active site and then continued with building its pharmacophore model, which would be employed to screen compounds obtained from the Zinc database. Subsequently, the best compound derived from this pharmacophore model analysis was docked onto the PfDHFR-TS receptor, which also evaluated its binding energy and chemical interactions. The compounds identified as the most promising candidates through the screening process were further assessed *in silico* for their ADMET-drug likeness parameter, and their complex stability was evaluated using molecular dynamic simulations.

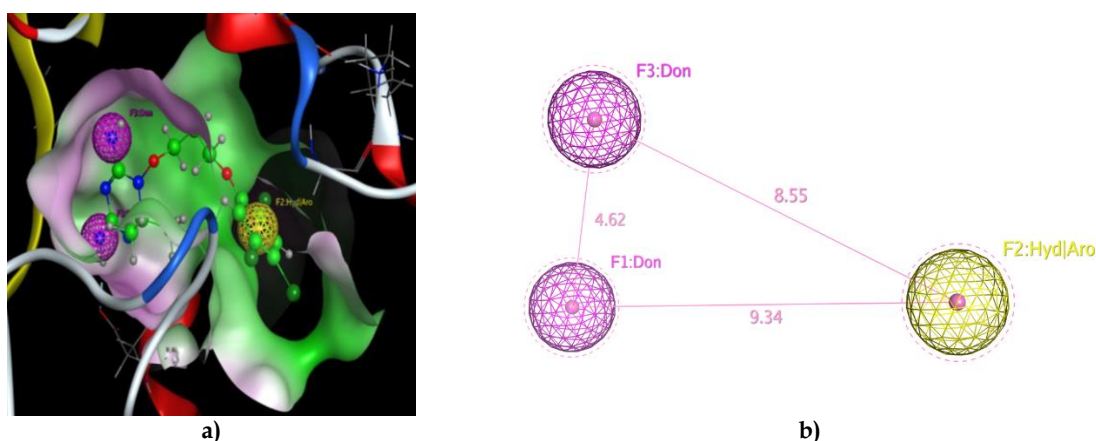


Figure 1. Validated pharmacophore model with appearance in binding pocket of the receptor (a), validated pharmacophore features (b).

2. RESULTS and DISCUSSION

2.1. Pharmacophore model generation and validation

The WR99210 compound is a potential native ligand and DHFR inhibitor that has been proven to inhibit quadrupole mutant PfDHFR and holds promise as a model for antimalarial drug-candidate development [16]. Ile14, Asp54, and Leu164 were among the important amino acids that formed bonds with the amino group of the WR99210 triazine ring during observations of crucial interactions between WR99210 and the binding

pocket of quadrupole mutant P β DHFR (PDB ID 1j3k) [17], while the benzene ring facilitated hydrophobic interactions with Leu46, Phe58, and Ile112. Next, using the results of this study as a guide, a pharmacophore model was created by adding a number of important functional groups from WR99210 to get pharmacophore features (Figure 1). It was found that there are two important pharmacophores: one with a hydrophobic/aromatic feature (F2: Hyd/Aro, yellow color) and two with hydrogen bond donor features (F1 and F3: Don, purple color) (Figure 1b). As confirmed in Figure 1a, the F1 and F3 features, located on the substituted amino group of the triazine ring, form interactions with Ile14, Asp54, and Leu164, while the F2 feature, positioned on the aromatic ring, interacts with Leu46, Phe58, and Ile112.

To ensure the reliability of the pharmacophore model, validation was performed using the enrichment factor (EF), the Guner-Henry (GH) parameter, and the receiver operating characteristic (ROC). A total of 1004 compounds from the database were screened and evaluated using the pharmacophore model. Based on Table 1, this pharmacophore model was capable of identifying nearly 80% of active compounds, with an enrichment factor of 20.35. Next, the GH value obtained was 0.8, which indicates that this pharmacophore model has good capabilities for identifying hit compounds in the database and is suitable for use in virtual screening. The validation of the pharmacophore model using receiver operating characteristic (ROC) analysis aims to determine its ability to distinguish active compounds from decoy ones. An AUC value greater than 0.7 is considered indicative of a good model [18]. As illustrated in Figure 2, this model exhibits an AUC value of 0.89. This, coupled with its high sensitivity (%Se) and specificity (%Sp) of over 80%, as shown in Table 1, demonstrated the model's utility for further virtual screening as well.

Table 1. Derivatives of new pyrimidine compounds and predicted MIC values.

No	Parameter	Value
1	Total molecule in data base (D)	1004
2	Total number of actives in database (A)	39
3	Total hits (Ht)	43
4	Active hits (Ha or Tp)	34
5	%yield of active ((Ha/Ht)x100)	79.07
6	%ratio of active ((Ha/A)x100)	87.18
7	Enrichment factor (E) ((Ha x D)/(Ht x A))	20.35
8	False negative (A-Ha)	5
9	False positive (Ht-Ha)	9
10	True negative	815
11	Se%	87.18
12	Sp%	98.91
13	Goodness of hit score (GH)	0.80

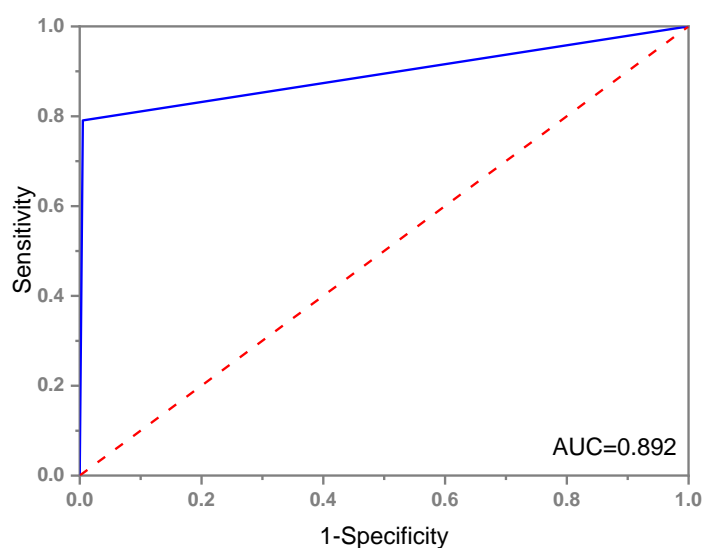


Figure 2. Pharmacophore validation based on receiver operating characteristic (ROC).

2.2. Virtual screening uses a pharmacophore model

The validated pharmacophore model was employed for virtual screening. A total of 165,8778 purchasable compounds from the Zinc database were mapped to the validated pharmacophore model features. Low RMSD values indicated that hit compounds had the best overlap in these features. Further, to reduce the number of hit compounds obtained, the RMSD value threshold was set to less than 0.5 Å. At this stage, 500 compounds were obtained and were subsequently subjected to molecular docking against the quadrupole mutant PfdHFR.

2.3. Molecular docking

At this stage, molecular docking of the 500 compounds obtained from virtual screening yielded the top 10 most favorable compounds. Afterwards, these compounds were re-docked using an exhaustiveness parameter, resulting in the identification of the five best compounds which were heterocyclic compound derivatives, as depicted in Figure 3. These 5 compounds exhibited binding energies ranging from -40 to -42 kJ/mol, surpassing the binding energy of the native ligand. As shown in Table 2, compound C431 exhibited the highest binding energy (-42.26 kJ/mol), followed by compound C358 and C445 (-41.00 kJ/mol). Low binding energy indicates that the compounds have the potential to form a stable complex with the receptor.

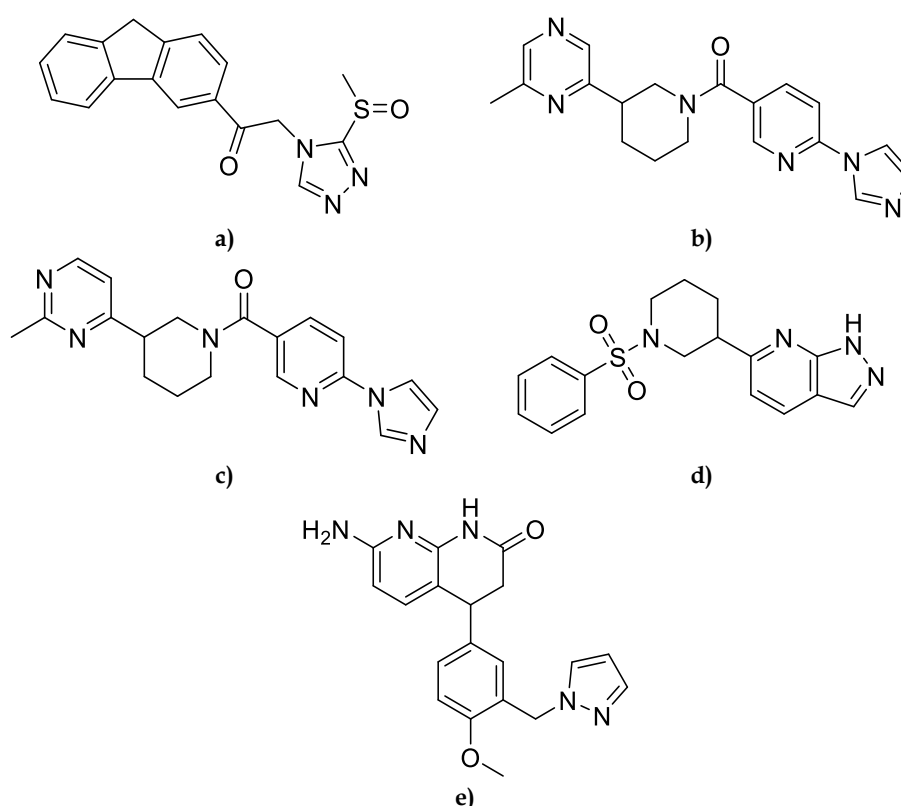


Figure 3. Proposed compounds obtained by virtual screening: compound C313 (a), compound C328 (b), compound C358 (c), compound C431 (d), compound C445 (e).

Interactions of the five best compounds within the binding pocket of the PfdHFR mutant quadrupole receptor were evaluated and compared to those of WR99210, as illustrated in Figure 4. The compound C313 had the lowest binding energy (-40.17 kJ/mol) and the complex was held together only by hydrophobic interactions at Met55 and Leu46. Further, compound C328 shared the same binding energy as compound C313. However, it additionally formed a hydrogen bond with Ile 14. Based on the observation, the interaction distance in this hydrogen bond was quite large compared to the interaction distances in hydrogen bonds of native ligand compounds with similar bond types. Moreover, compound C358 had a slightly higher binding affinity than the earlier-mentioned two compounds. The evaluation results showed that the compound C358 stabilized by hydrophobic interactions with amino acid residues Leu46, Phe58, and Ile112 binds to the receptor binding pocket via a hydrogen bond with Ile14 [19].

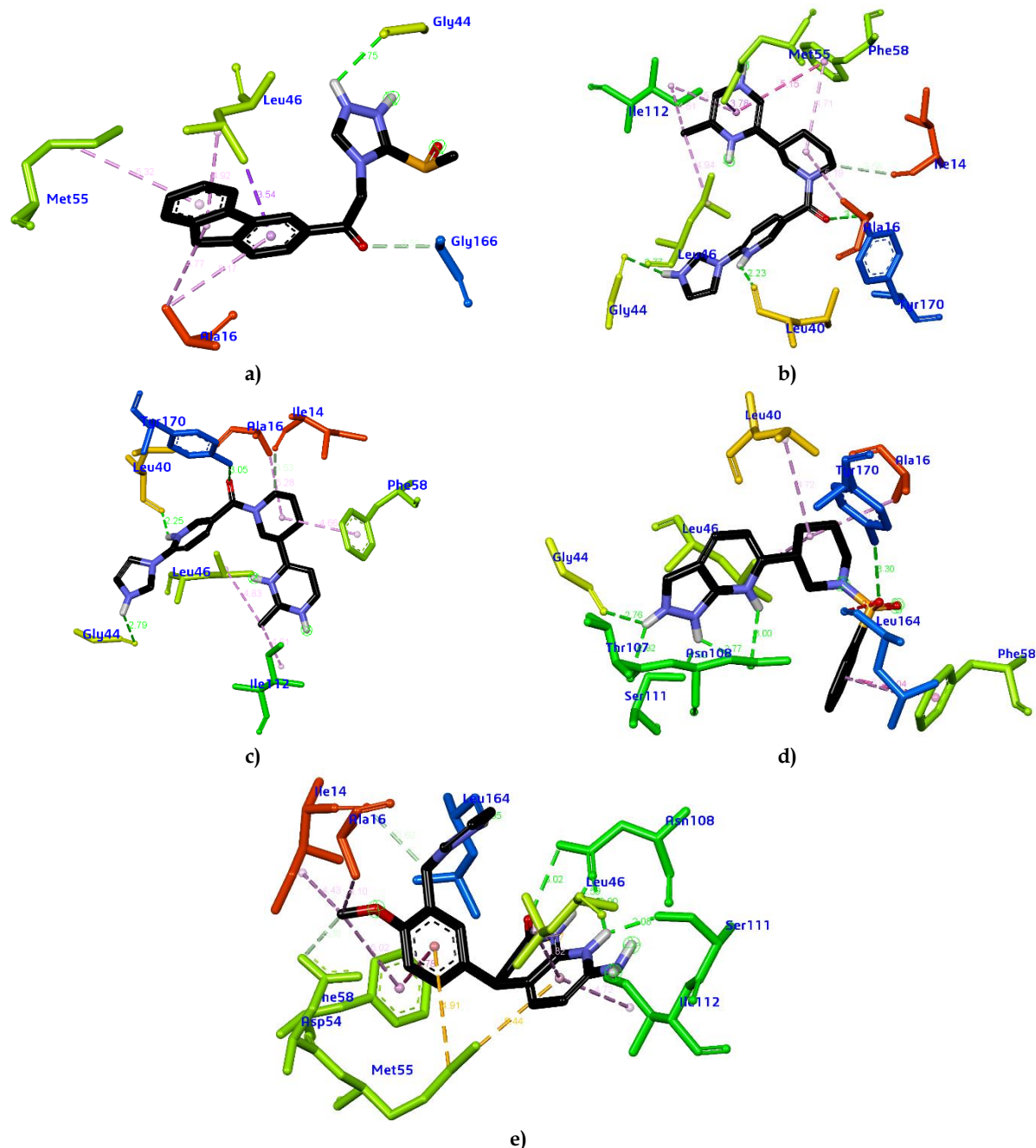


Figure 4. Three-dimensional visualization of chemical interactions between hit compounds and the quadrupole binding pocket of *PfDHFR* mutants: Compound C313 (a), Compound C328 (b), Compound C358 (c), Compound C431 (d), Compound C445 (e).

An interesting observation was made in two other compounds, specifically compounds C445 and C431. First, the compound C431 exhibited the highest binding affinity (-42.26 kJ/mol). The results of the interaction evaluation showed that compound C431 could form a hydrogen bond with Ser111 with a shorter bond length (1.92 Å) compared to the bonds in compound WR99210. Furthermore, compound C431 could stabilize its complex by engaging in alkyl and pi-pi stacked interactions in Leu46 and Phe58, respectively. Secondly, compound C445 exhibited a lower binding energy than compound C431, but its interaction model closely resembled that of compound WR99210. The compound C445 formed hydrogen bonds with Ile14, Asp54, Ser111, and Leu164 residues, while hydrophobic interactions were observed with Leu46, Met55, Phe58, and Ile112 [7].

Table 2. Binding energy and chemical interaction of the hit compound with quadrupole mutant PfDHFR.

ID Compound	ID Zinc Database	IUPAC name	Binding energy (kJ/mol)	Pharmacophore RMSD	Interaction		
					Hydrogen bond	Distance (Å)	Hydrophobic
WR99210	-		-35.98	-	Ile14 Cys15 Asp54 Ser111 Leu164	2.10 2.58 2.45 2.97 2.06	Val45, Leu46, Met55, Phe58, Ile112, Pro113, Phe116
C313	ZINC96447742	(1-(9H-fluoren-3-yl)-2-[3-[(S)-methylsulfinyl]-1,2,4-triazol-4-yl]ethanone)	-40.17	0.079	Gly44 Gly166	2.75 3.59	Ala16, Met55, Leu46
C328	ZINC257232119	((6-imidazol-1-ylpyridin-3-yl)-[(3R)-3-(6-methylpyrazin-2-yl)piperidin-1-yl]methanone)	-40.17	0.081	Ile14 Leu40 Gly44 Tyr170	3.58 2.23 2.77 3.02	Ala16, Leu46, Met55, Phe58, Ile112
C358	ZINC257251352	((6-imidazol-1-ylpyridin-3-yl)-[(3R)-3-(2-methylpyrimidin-4-yl)piperidin-1-yl]methanone)	-41.00	0.083	Ile14 Leu40 Gly44 Tyr170	3.53 2.25 2.79 3.05	Ala16, Leu46, Phe58, Ile112
C431	ZINC257280996	(6-[(3R)-1-(benzenesulfonyl)piperidin-3-yl]-1H-pyrazolo[3,4-b]pyridine)	-42.26	0.087	Gly44 Thr107 Asn108 Ser111 Tyr170	2.76 2.82 2.77 1.92 3.30	Ala16, Leu40, Leu46, Phe58
C445	ZINC91644095	4-(3-((1H-pyrazol-1-yl)methyl)-4-methoxyphenyl)-7-amino-3,4-dihydro-1,8-naphthyridin-2(1H)-one	-41.00	0.089	Ile14 Asp54 Asn108 Ser111 Leu164	3.69 3.36 1.59 2.08 1.95	Ala16, Leu46, Met55, Phe58, Ile112

The results shown in Table 2 show that pharmacophore mapping of the five best compounds gave acceptable RMSD values below 0.1 Å. This shows that the high binding energy of each compound is related to this. Further analysis revealed that pharmacophore features in each compound contribute to crucial interactions with the receptor's binding pocket. Figure 5 illustrates the pharmacophore feature mapping of each compound. The F2 hydrophobic-aromatic feature was detected in compound C313, while compound C328 interacted with Leu46. The F3 hydrogen donor feature in compound C328 enabled carbon-hydrogen bond interactions at Ile14. This was because this type of interaction was not sufficient to stabilize the complex and caused low binding energy. In contrast, compound C358 possessed a structure resembling that of compound C328. However, the N atom was positioned on a distinct bipyridine ring. Moreover, the pharmacophore features of compound C358 were also found to be identical to those of compound C328; consequently, the available interaction types were also identical. In compound C431, the F3 hydrogen donor feature was found on the pyridine carbon, which facilitated stacked pi-pi and alkyl interactions on Leu46, while the hydrogen bond interaction on Leu164 by compound C445 was found in the F2 feature hydrophobic-aromatic.

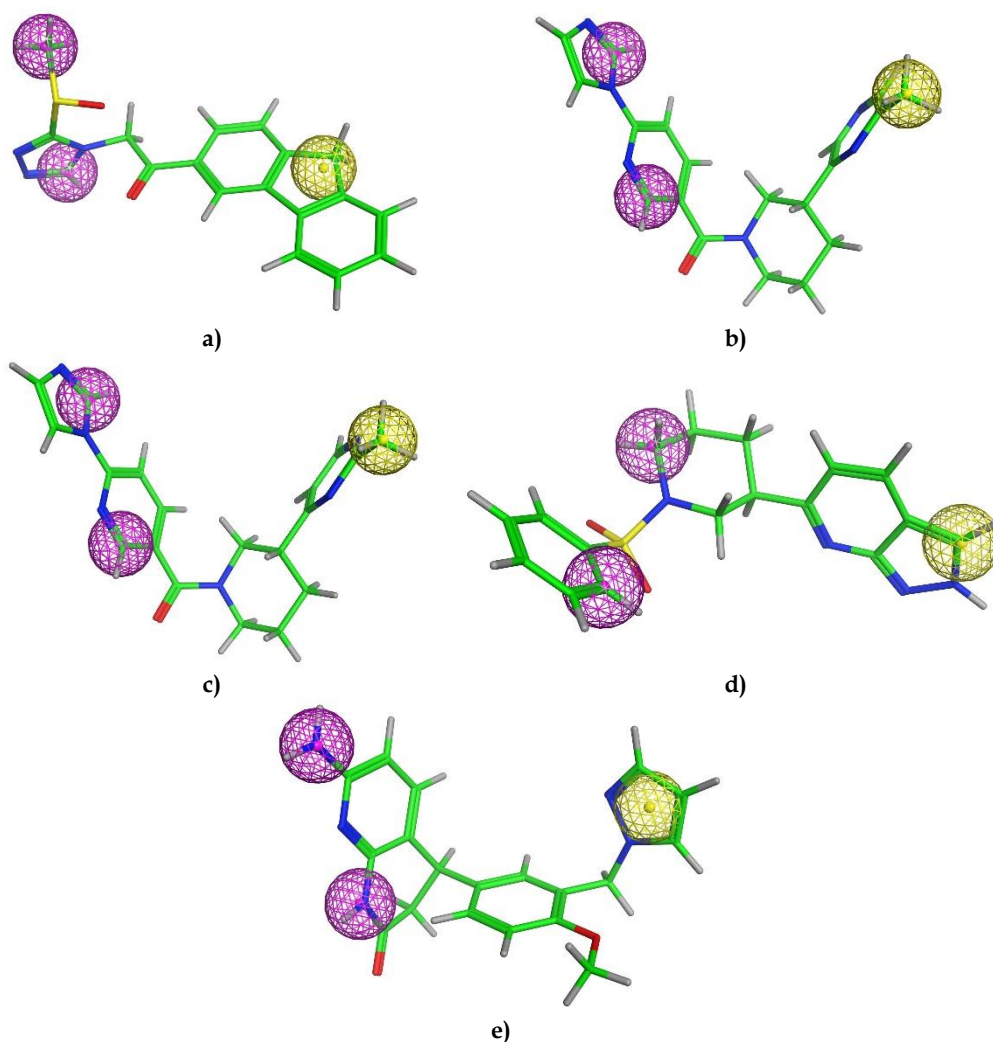


Figure 5. Visualization of pharmacophore mapping of proposed compounds: Compound C313 (a), Compound C328 (b), Compound C358 (c), Compound C431 (d), Compound C445 (e).

Table 3. ADMET properties of the most promising compounds identified through screening.

	C313	C328	C358	C431	C445
Absorption					
Intestinal absorption (%)	99.27	98.80	98.75	95.00	88.85
Caco2 permeability (nm sec ⁻¹)	1.34	1.41	1.43	1.16	0.84
Distribution					
Volume of distribution (log L Kg ⁻¹)	-0.21	0.05	0.05	0.29	-0.05
Blood-brain barrier (log BB)	0.29	-1.14	-1.14	-1.33	-0.53
Central nervous system (log PS)	-2.53	-2.97	-2.98	-4.09	-2.69
Metabolism					
CYP2D6 substrate (Yes/No)	No	No	No	No	No
CYP3A4 substrate (Yes/No)	Yes	No	No	Yes	Yes
CYP2D6 inhibitor (Yes/No)	No	No	No	No	No
CYP3A4 inhibitor (Yes/No)	No	No	No	No	No
Excretion					
Total clearance (log mL min ⁻¹ Kg ⁻¹)	0.19	0.59	0.50	0.84	0.33
Toxicity					
AMES toxicity (Yes/No)	Yes	Yes	Yes	No	No

2.4. ADMET and Drug-likeness analysis

In many cases, it has been observed that the failure of a compound developed in the drug development phase is due to suboptimal ADME and associated toxicities. In this study, the ADME and toxicity properties of the five most favorable compounds were evaluated using the pkCSM web tool to identify and eliminate

compounds with suboptimal ADMET profiles. Firstly, absorption describes the process by which a drug is taken up into the body through oral administration [20]. As detailed in Table 3, all compounds exhibited favorable intestinal absorption except for compound C445, which fell below 90%. Based on their chemical structures, these five compounds possessed functional groups that facilitated both hydrogen bond acceptor and hydrogen bond donor interactions. As a consequence, they exhibited improved water solubility. The Caco2 permeability parameter study also showed results that were similar to the intestinal absorption data, except for compound C445, which had values below 0.90 nm sec⁻¹. This parameter becomes an *in vitro* model for predicting whether a drug can be given orally [21].

Secondly, distribution properties are essential pharmacokinetic properties that play a crucial role in determining whether a compound can exhibit its efficacy or not after the absorption phase. The volume of distribution (VD_{ss}) is a value that reflects the tendency of a compound to bind into the blood plasma rather than tissues. When the compound binds more strongly to blood plasma, the VD_{ss} is greater than 0.45 [22], indicating that the compound may fail to exhibit its efficacy. The results of the study demonstrated that all five compounds exhibited VD_{ss} values below 0.45, indicating that these favorable compounds are likely to retain efficacy. Moreover, the results of the blood-brain barrier (BBB) and central nervous system (CNS) permeability studies revealed that all tested compounds exhibited low values for these parameters. Consequently, it was predicted that all compounds would be unable to permeate through the brain membranes and CNS [23].

Third, studying how these compounds are broken down showed that compounds C313, C431, and C445 might be able to bind to CYP3A4. Cytochrome P450 enzymes (CYP2D6 and CYP3A4) are very important for breaking down and getting rid of xenobiotics from the body. This helps lower the risk of bad drug reactions and drug toxicity [24]. Finally, regarding excretion and toxicity, compound C313 exhibited the lowest overall clearance value. The AMES test results supported this fact by suggesting that compound C313 might have reduced clearance and possibly cause toxicity. Contrariwise, compound C431 exhibited the highest overall clearance value (0.84 log mL min⁻¹ Kg⁻¹), followed by compounds C328, C358, and C445, respectively. However, only compounds C431 and C445 were found to be non-toxic based on the AMES toxicity evaluation.

Table 4. Drug-likeness properties of the top five candidate compounds

Compound	^a Molecular Weight (MW)	^a Log P	^a Number of HBA	^a Number of HBD	^a PSA (Å ²)	Violation of Lipinski rule	^b Drug-likeness score
C313	337.40	1.42	4	0	84.06	-	-0.06
C328	348.40	2.62	5	0	76.80	-	0.07
C358	348.40	2.78	5	0	76.80	-	0.28
C431	342.42	1.87	5	1	87.33	-	0.31
C445	349.39	2.18	4	2	95.06	-	0.79

^acalculated by SwissAdme, ^bcalculated by Molsoft webtools

The drug-likeness properties of the top five compounds were evaluated based on the Lipinski rule. This evaluation was conducted to assess whether these compounds, which were shown to inhibit the quadrupole mutant PfDHFR *in silico*, could be administered orally as drugs. As described in Table 4, all these compounds did not break the Lipinski rule. Thus, they have promising antimalarial drug-candidates as they have a molecular weight (MW) of no more than 500, a log P value of less than 5, number of hydrogen bond acceptors (HBA) of no more than 10, number of hydrogen bond donors (HBD) of no more than 5, and polar surface area (PSA) of no more than 140 Å² [25,26]. Furthermore, the results of drug-likeness calculations using Molsoft web tools exhibited that compound C445 had the best drug-likeness score of 0.79. Therefore, by comparing with the previous ADMET data (Table 3), compound C445 along with C431 exhibited better ADMET characteristics than the other three compounds. It can be concluded that these two compounds have the potential to be developed further.

2.5. Molecular dynamics simulation

To gain valuable insight about the complex stability of C431 and C445, molecular dynamics simulation over 100 ns was performed. The complex stability of WR99210 in PfDHFR was also evaluated for comparison. Root mean square deviation (RMSD) describes the movement deviation of the conformation structure that compares to the initial conformation structure. Figure 6a shows the RMSD backbone of the protein. Complex C431 and C445 exhibited a stable RMSD value from initial to 20 ns, with RMSD values around 0.21 and 0.19 nm, respectively. Nonetheless, after 20 ns of simulation, both complexes demonstrated a fluctuating RMSD value. It is supposed that the flexibility of the protein, namely residues 25–90, is attributed to the decreased

interaction of both compounds. The complexes C431 and C445 were equilibrated when simulation entered 80 ns with a mean rmsd value of 0.19 nm and 0.22 nm, respectively. Meanwhile, complex WR99210 showed stability from 20 ns to end with a mean rmsd of 0.21 nm.

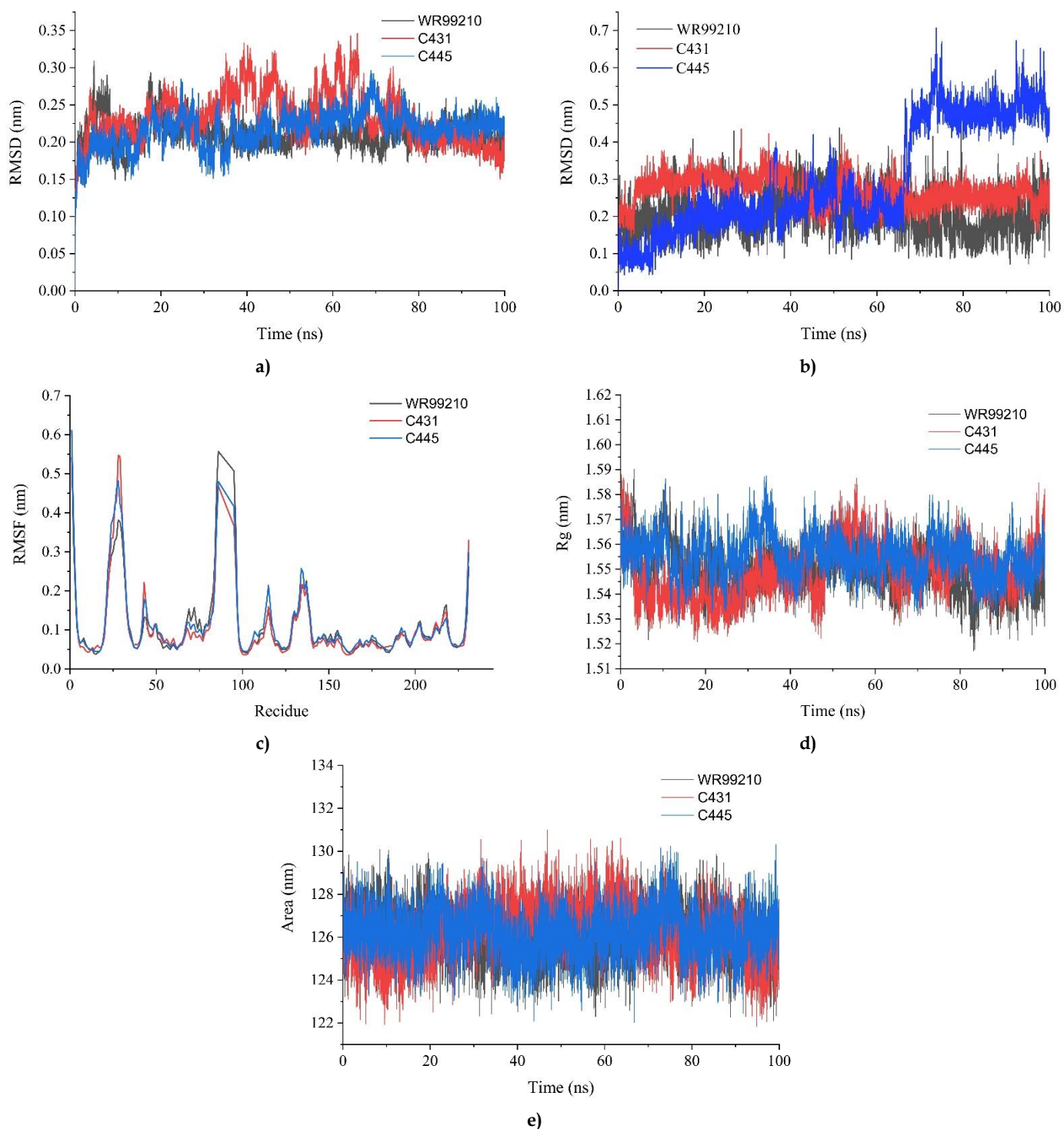


Figure 6. MD simulation visualization of native ligand, compounds C431, and C445: RMSD backbone (a), RMSD Ligand to Protein (b), RMSF (c), Radius of gyration (d), SASA (e).

The stability of each compound at the binding site was studied and presented as RMSD ligand fit to protein (Figure 6b). Compounds C445 and WR99210 displayed increased RMSD at initial to 22 ns. Moreover, compound WR99210 showed a stable pattern until the end of the simulation with an RMSD value of 0.20 nm, while the RMSD value of compound C445 spurted to 0.51 nm at 65 ns simulation. This indicates that compound C445 is more unstable than compound C431. The flexibility of each residue amino acid is presented

in the root mean square fluctuation (RMSF) plot (Figure 6c). Several amino acid residues in the binding pocket, such as Ile14, Asp54, Ser111, and Leu164 for both complexes, showed RMSF values below 2 Å (0.2 nm). This indicates that the ligand-interacting amino acid residues exhibit rigidity [27]. Thus, the ligand interaction within the active site of the protein binding pocket has achieved stability. The mean RMSF for compounds WR99210, C431, and C445 is 0.10, 0.10, and 0.11 nm, respectively.

The other parameters used to explain the complex stability are the radius of gyration (Rg). The Rg plot provides information about the compactness of the receptor protein. As shown in Figure 6d, the protein in complex WR99210 is the stiffest of all the complexes. This indicated that the folded effect of this protein is minimal and compound WR99210 is likely to have interacted with the binding site [28]. When we compared the average Rg values of complexes C431 and C445, we discovered that complex C431 had a lower Rg value than complex C445. This implied that compound C431 was restrained at the binding site. Furthermore, solvent-accessible surface area (SASA) analysis of three complexes is performed to better understand the stability of compounds in residue amino acids as facilitated by hydrophobic interaction in the water system [27]. The mean SASA for compounds WR99210, C431, and C445 is 126.11, 126.20, and 126.21 nm, respectively. Compound C431 had a slightly lower average SASA than compound C445. This revealed that compound C431 is stable at the binding site but has a lower affinity for water molecules.

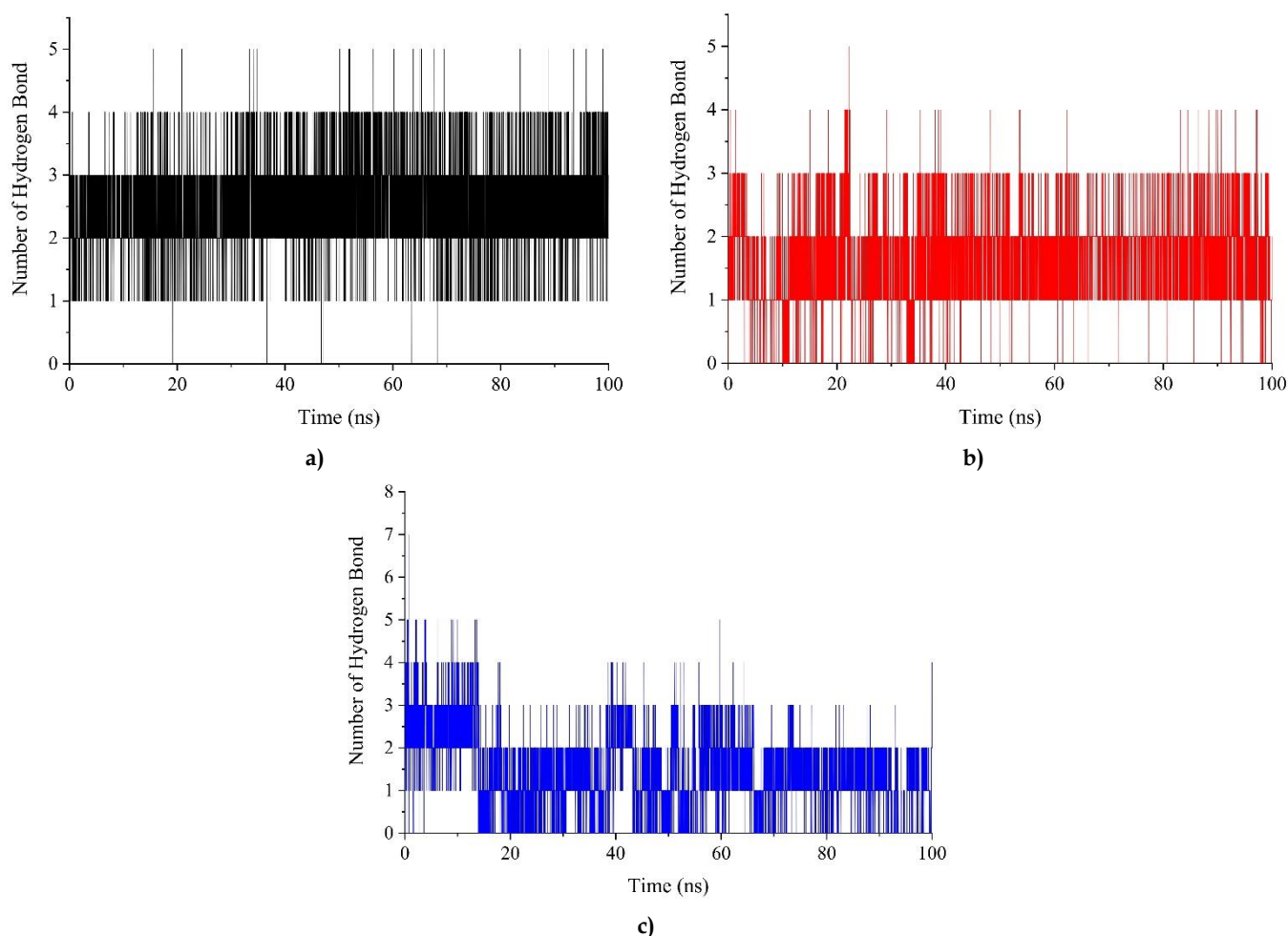


Figure 7. Number of hydrogen bondings obtained protein with native ligand (a), compound C431 (b), compound C445 (c).

The other interaction that contributes to the complex's stability is the hydrogen bond [27,29]. As illustrated in Figure 7, this information is presented as the total hydrogen bond obtained through simulation. Compound WR99210 has 1-4 total hydrogen bonds throughout the simulation. The total hydrogen bond of compound C445 was discovered at 0-4 for the first 15 ns, then decreased to 0-2. This indicated that an increase in the RMSD value of the ligand fit protein occurred (Figure 6b). As a result, compound C445 is losing stability in its complex. In contrast to compound C431, we discovered that compound C431 maintained a 0-3 hydrogen bond throughout the simulation. Simulation dynamics results were consistent with molecular docking

analysis. This indicates that compound C431 is the most stable and has the lowest binding energy of the compounds tested.

2.6. DFT study

The electronic parameters of compounds C431 and C445 were calculated through DFT studies. Electronic parameter calculations are aimed at predicting the reactivity and stability of proposed compounds and elucidating their biological activity. Initially, compounds C431 and C445 were subjected to geometric optimization using the Becke's Three-Parameter Lee-Yang Parr (B3LYP) method with a basis set of 6-311G(d). Subsequently, by using the optimized compounds (Figures 8a and 9a), their quantum chemical parameters were determined with several parameters as presented in Table 5. The highest occupied molecular orbital (HOMO) represents the ability of an optimized compound to donate electrons, while the lowest unoccupied molecular orbital (LUMO) reflects the ability of an optimized compound to absorb electrons. The HOMO and LUMO parameter values are used to determine the energy gap ($\Delta E = E_{LUMO} - E_{HOMO}$). The analysis results revealed that compound C431 exhibited a marginally smaller energy gap compared to compound C445, implying a higher reactivity of compound C431 relative to compound C445 (tends to be stable) [30]. This data exhibits a direct correlation with the binding energy data (Table 2), demonstrating that the compound C431 possessed a higher binding energy value compared to compound C445.

Table 5. Chemical quantum parameters of the best compounds

Quantum chemical parameter	Compound C431	Compound C445
HOMO (E_{HOMO} , eV)	-0.209	-0.202
LUMO (E_{LUMO} , eV)	-0.061	-0.025
Energy gap (ΔE , eV)	0.148	0.178
Ionization potential (I, eV)	0.209	0.202
Electron affinity (A, eV)	0.061	0.025
Hardness (η , eV)	0.074	0.089
Softness (σ , eV ⁻¹)	6.755	5.613
Electronegativity (χ , eV)	0.135	0.114
Electrophilicity (ω , eV)	0.124	0.073

The following are some quantum chemical parameters determined using the Koopmans theorem [31]. Firstly, the ionization potential (I) of compound C431 was found to be slightly larger (0.209 eV) than that of compound C445 (0.202 eV). This implies that compound C431 required a greater energy input to remove electrons from the molecule's ground state, suggesting a higher stability of compound C431 compared to compound C445. Secondly, in terms of electron affinity (A), compound C431 exhibited a higher A value compared to compound C445, implying its tendency to absorb electrons and be more reactive.

Thirdly, the next parameters that exert an influence on the stability and reactivity of a compound are hardness (η) and softness (σ). The compound C445 exhibited higher hardness properties compared to the compound C431. The hardness properties affect the resistance of an electron to be distributed throughout the molecule. Therefore, compound C445 tends to be more stable than compound C431. High softness implies a high propensity for reactivity in a compound [30]. Thus, compound C431 was more reactive than compound C445. Fourthly, in terms of electronegativity (χ), compound C431 exhibited a higher electronegativity, indicating a stronger affinity for attracting electrons compared to compound C445. Conversely, compound C445 demonstrated a tendency to absorb electrons, as evidenced by its electrophilicity value of 0.073 eV.

Visualization of the Frontier Molecular Orbitals (FMOs) from compounds C431 and C451 is depicted, respectively, in Figures 8c and 9c. In compound C431, the HOMO delocalization area was found to be on the H-pyrazole [3,4-b] pyridine ring, and the LUMO delocalization area was found to be on the benzene-sulfonyl moiety. As it was explained, the HOMO region tended to donate electrons. The molecular docking of compound C431 showed that the H-pyrazole [3,4-b] pyridine structure connected to Ser111 and Asn108 through hydrogen bonds. Furthermore, the benzene-sulfonyl structure in the LUMO region exhibited a tendency to accept electrons and was found to engage in hydrophobic interactions with Phe58. Second, in compound C445, the HOMO region was inside the structure of 3,4-dihydro-1H-1,8-naphthyridin-2-one. It helped form important hydrogen bonds in Ser111 by donating an electron and making it easier for hydrophobic interactions to happen with Leu46, Ile112, and Met55. While the LUMO region exhibited interactions analogous to those observed in the HOMO region.

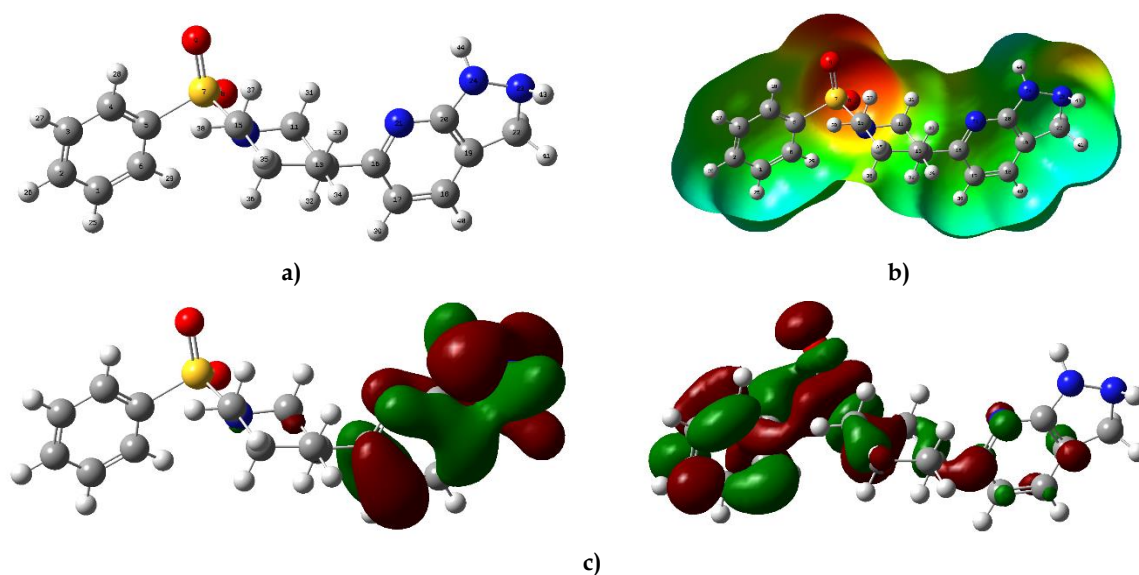


Figure 8. Visualization from C431 optimized structure (a), MEP (b), energy gap of HOMO (Left) and LUMO (Right) (c).

Molecular electrostatic potential (MEP) provides insights into the charge distribution of a compound and reveals its reactivity side location, both the nucleophilic and the electrophilic side. Most importantly, this information can be harnessed to deepen the understanding of hydrogen bonding interactions between ligands and receptors. In this research, the molecular electrostatic potential (MEP) of compound C431 and compound C445 has been studied, as depicted in Figures 8b and 9b. The MEP of these compounds showed that the oxygen (O), sulfur (S), and nitrogen (N) atoms appeared as red and yellow, while the aromatic group was shown in green. The red and yellow colors indicate the nucleophilic side, which provides hydrogen bond interaction, while the green one exhibits the electrophilic side. The electrophilic region serves as the site of nucleophilic attack, mediated by hydrophobic interactions with the amino acid residue on the receptor. This MEP visualization provides evidence corroborating the presence of hydrogen bonds and hydrophobic interactions observed in molecular docking studies.

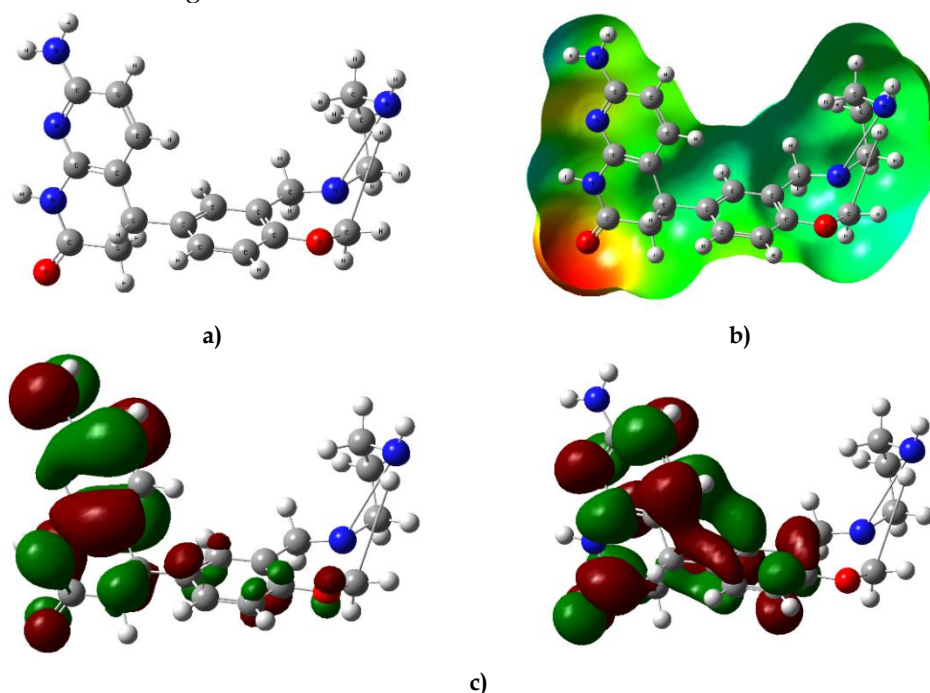


Figure 9. Visualization from C445 optimized structure (a), MEP (b), energy gap of HOMO (Left) and LUMO (Right) (c).

3. CONCLUSION

Structure-based pharmacophore, molecular docking, and molecular dynamics have been used to find compounds that might be good at fighting malaria. Screening of 165,878 purchasable compounds from the Zinc database found the five best compounds with binding energies of -40.17 to -42.26 kJ/mol. These binding energies are higher than those of the control compound, WR99210. Among these five best compounds, compounds C431 and C445 emerged as the most promising candidates due to their favorable ADME properties and non-toxic nature. Evaluation of the complex stability of compounds C431 and C445 through molecular dynamics simulations showed that compound C431 had a stable complex during 50 ns of simulation, and based on quantum calculations using DFT studies, compound C431 had reactive properties. Finally, the results of this in silico study suggest that compound C431 is a promising antimalarial candidate. However, further studies are needed to synthesize the compound and test its antimalarial activity in the laboratory.

4. MATERIALS AND METHODS

4.1. Materials

This study utilized a combination of software programs, encompassing: ChemOffice Professional 16, ChemD3, Autodock Vina, Autodock Tools (ADT), Molecular Operating Environment (MOE) 2015, Discovery Studio Client 2021 version 21.1.0.20298, and Gaussian 9. All of these applications were run on hardware with a Core i9-13900H processor and 16 GB of RAM windows 10 operating system.

4.2. Pharmacophore model generation and validation

Initially, a pharmacophore model was constructed using a structure-based design approach, employing the structure of the quadrupole mutant PfDHFR as a receptor with PDB code 1j3k, retrieved from the RSCB website. Subsequently, the quadrupole mutant structure of PfDHFR was minimized using MOE with the MMFF94X force field parameters. The chemical interactions of WR99210, a native ligand in the receptor binding pocket, were analyzed to develop pharmacophore features using MOE. Eventually, the pharmacophore model that had been constructed was validated using 1004 compounds, which contain 39 active and 965 decoy compounds, and was also evaluated based on Güner-Henry (GH), enrichment factor (EF), and receiver operating characteristic (ROC) parameters [32]. For the records, active compounds were adopted from the ChEMBL database (<https://www.ebi.ac.uk/chembl/>) while the decoy ones were retrieved from the Dekois website (<https://www.pharmchem.uni-tuebingen.de/dekois/>) [33,34].

4.3. Virtual screening using pharmacophore models

A total of 165,878 purchasable compounds gathered from the Zinc database were utilized as the data set for screening against a validated pharmacophore model. First, the MMFF94X force field parameters were used to minimize the structures of the compounds in the data set. Next, MOE was used to add hydrogen atoms and partial charges. Afterwards, these compounds were screened using a validated pharmacophore model. The results were evaluated by calculating root mean square deviation (RMSD) values, which reduces the hit compounds obtained. The RMSD threshold value was adjusted below 0.5 Å [35]. Finally, compounds that passed this stage of screening were subsequently subjected to molecular docking simulations.

4.4. Molecular docking

A total of 500 compounds that passed the threshold following screening using a pharmacophore model were investigated for their inhibitory activity against the quadrupole mutant PfDHFR through molecular docking simulations. Firstly, the docking protocol validation was executed by redocking the native ligand against the pocket-binding receptor. At this stage, the native ligand was prepared by adding hydrogen atoms and the Gasteiger charge. It was then saved in pdbqt format. Meanwhile, the receptor preparation was completed by adding polar hydrogen atoms and the Kollman charge. It was also saved in pdbqt format. As a result, the docking protocol with an RMSD value of <1 Å was considered valid and could be effectively utilized for screening purposes [36]. Secondly, molecular docking simulations for 500 compounds were carried out using AutoDock Vina, employing a box size of 12 × 16 × 18 Å and centers of x, y, and z at 28.85, 6.56, and 58.89, respectively, with an energy range of 4. In the next step, the top 10 compounds with the most favorable binding energy (kJ/mol) underwent geometric optimization using the Austin Model 1 (AM1) method implemented in Gaussian 09 software. These 10 compounds were subsequently re-simulated using molecular docking with AutoDock Vina, employing the same box size and center values as the previous one but with an exhaustiveness of 100. Finally, adhering to the aforementioned process, the five compounds with the most

favorable binding energy were selected, followed by analyzing and visualizing their chemical interactions using Biovia Discovery Studio 2021 version 21.1.0.20298.

4.5. ADMET and drug-likeness analysis

The 5 compounds selected earlier were analyzed for their ADMET properties by inputting their respective SMILES data into the pkCSM web tool (<https://biosig.lab.uq.edu.au/pkcsm/prediction>), while their drug-likeness properties were determined and evaluated using the SwissADME webserver (<http://www.swissadme.ch/>) as well as Lipinski's rule. Moreover, drug-likeness values were calculated using the Molsoft web server (<https://molsoft.com/mprop/>).

4.6. Molecular dynamics simulation

We looked at two compounds that had the best binding energy based on molecular docking predictions and ADMET-drug likeness properties. We then tested how stable their interaction was in the binding pocket of the quadrupole mutant PfDHFR using molecular dynamics simulations with the Gromacs 2023 package [37]. Initially, the ligand topology was created utilizing acpype with the General AMBER force field (GAFF2) [38]. The receptor topology was prepared using Gromacs, employing the AMBER99SB force field [39], and TIP3P as the water model [40]. The neutralization process was executed by adding Na⁺ and Cl⁻ ions to the ligand-protein structure, which had been previously shaped into a dodecahedron and filled with water molecules. The system was optimized via steepest descent minimization. The system was then equilibrated under NPT and NVT conditions for 1000 ps at a temperature of 300 kelvin. Following that, a 100 ns molecular dynamics production was performed at a pressure of 1 bar and a temperature of 300 K. Finally, the simulated trajectory obtained from this process is used for analyzing the RMSD, RMSF, the number of hydrogen bonds formed between the ligand and the protein, Rg, and SASA.

4.7. DFT study

Geometry optimization of the two most favorable compound structures was performed using B3LYP method with a 6-311G basis set. The structure compounds were optimized using Gaussian 09 software. In addition, the molecular electrostatic potential (MEP) map of each structure was visualized using GaussView 06, and the Koopman value was calculated to determine quantum chemical parameters such as energy gap (ΔE), ionization potential (I), electron affinity (A), electronegativity (χ), chemical potential (μ), hardness (η), softness (σ), and electrophilicity (ω) [41].

This is an open access article which is publicly available on our journal's website under Institutional Repository at <http://dspace.marmara.edu.tr>.

Acknowledgements: The author acknowledges the Ministry of Health Republic Indonesia for their financial support in conducting a research project in collaboration between the Health Polytechnic of Kupang and Management and Science University (MSU), as outlined in agreement number HK.02.03/1/4376/2023.

Author contributions: Concept - P.J.P.T.; Design - P.J.P.T., F.O.N.; Supervision - F.O.N., D.M., M.H.; Resources - P.J.P.T., M.H.; Materials - S.B.M.A.W.; Data Collection and/or Processing - O.S.S.; Analysis and/or Interpretation - P.J.P.T., F.O.N.; Literature Search - P.J.P.T., F.O.N. D.M., S.V.N., I.A.; Writing - P.J.P.T., F.O.N.; Critical Reviews - P.J.P.T., S.V.N., F.O.N., D.M., O.S.S., S.B.M.A.W., M.H., I.A., M.O.B

Conflict of interest statement: The authors declared no conflict of interest in the manuscript.

REFERENCES

- [1] Rosenthal PJ. Malaria in 2022: Challenges and Progress. *Am J Trop Med Hyg.* 2022; 106(6): 1565-1567. <https://doi.org/10.4269/AJTMH.22-0128>
- [2] World Health Organization. World Malaria Report 2022. https://www.mmv.org/newsroom/news-resources-search/world-malaria-report-2022?gclid=CjwKCAiArfauBhApEiwAeoB7qA6Q9Va01OF0B6gGWENAb9rsmOPmSPiRmH6lzSGoDI6_aR_otcoEaxoC3G4QAvD_BwE (accessed November 15, 2023).
- [3] Shibeshi MA, Kifle ZD, Atnafie SA. Antimalarial drug resistance and novel targets for antimalarial drug discovery. *Infect Drug Resist.* 2020; 13: 4047-4060. <https://doi.org/10.2147/IDR.S279433>
- [4] Sabe VT, Ntombela T, Jhamba LA, Maguire GEM, Govender T, Naicker T, Kruger HG. Current trends in computer aided drug design and a highlight of drugs discovered via computational techniques: A review. *Eur J Med Chem.* 2021; 224: 113705. <https://doi.org/10.1016/j.ejmech.2021.113705>
- [5] Surabhi S, Singh B. Computer Aided Drug Design: An Overview. *J Drug Deliv Ther.* 2018; 8(5): 504-509. <https://doi.org/10.22270/JDDT.V8I5.1894>

- [6] Muhammed MT, Aki-Yalcin E. Molecular docking: Principles, advances, and its applications in drug discovery. *Lett Drug Des Discov*. 2022; 21(3): 480–495. <https://doi.org/10.2174/1570180819666220922103109>
- [7] Singh IV, Mishra S. Molecular docking analysis of pyrimethamine derivatives with *Plasmodium falciparum* dihydrofolate reductase. *Bioinformation*. 2018; 14(05): 232–235. <https://doi.org/10.6026/97320630014232>
- [8] Hodoamede P. P. *falciparum* and its molecular markers of resistance to antimalarial drugs. In: Tyagi RK. (Eds). *Plasmodium Species and Drug Resistance*. IntechOpen, Inc., United Kingdom, 2021, pp.1-21.
- [9] Kreutzfeld O, Tumwebaze PK, Byaruhanga O, Katairo T, Okitwi M, Orena S, Rasmussen SA, Legac J, Conrad MD, Nsoya SL, Aydemir O, Bailey JA, Duffey M, Cooper RA, Rosenthal PJ. Decreased susceptibility to dihydrofolate reductase inhibitors associated with genetic polymorphisms in Ugandan *Plasmodium falciparum* isolates. *J Infect Dis*. 2022; 225(4): 696–704. <https://doi.org/10.1093/INFDIS/JIAB435>
- [10] Posayapisit N, Pengon J, Prommana P, Shoram M, Yuthavong Y, Uthaiyapibull C, Kamchonwongpaisan S, Jupatanakul N. Transgenic pyrimethamine-resistant *Plasmodium falciparum* reveals transmission-blocking potency of P218, a novel antifolate candidate drug. *Int J Parasitol*. 2021; 51(8): 635–642. <https://doi.org/10.1016/j.ijpara.2020.12.002>
- [11] Rastelli G, Sirawaraporn W, Sompornpisut P, Vilaivan T, Kamchonwongpaisan S, Quarrell R, Lowe G, Thebtaranonth Y, Yuthavong Y. Interaction of pyrimethamine, cycloguanil, WR99210 and their analogues with *Plasmodium falciparum* dihydrofolate reductase: Structural basis of antifolate resistance. *Bioorg Med Chem*. 2000; 8(5): 1117–1128. [https://doi.org/10.1016/S0968-0896\(00\)00022-5](https://doi.org/10.1016/S0968-0896(00)00022-5)
- [12] Tarnchompoo B, Chitnumsub P, Jaruwat A, Shaw PJ, Vanichtanankul J, Poen S, Rattanajak R, Wongsombat C, Tonsomboon A, Decharuangsilp S, Anukunwithaya T, Arwon U, Kamchonwongpaisan S, Yuthavong Y. Hybrid inhibitors of malarial dihydrofolate reductase with dual binding modes that can forestall resistance. *ACS Med Chem Lett*. 2018; 9(12): 1235–1240. <https://doi.org/10.1021/acsmmedchemlett.8b00389>
- [13] Borkakoty B, Sarma K, Parida P, Prakash A, Mohapatra P, Mahanta J. In silico screening of antifolate based novel inhibitors from *Brucea mollis* Wall. ex kurz against quadruple mutant drug resistant PfDHFR. *Comb Chem High Throughput Screen*. 2014; 17(8): 681–693. <https://doi.org/10.2174/1386207317666140521153305>
- [14] Da Silva RSFL, Olanda CG, Fokoue HH, Sant'Anna CMR. Virtual screening techniques in drug discovery: Review and recent applications. *Curr Top Med Chem*. 2019; 19(19): 1751–1767. <https://doi.org/10.2174/1568026619666190816101948>
- [15] Wang Z, Sun H, Shen C, Hu X, Gao J, Li D, Cao D, Hou T. Combined strategies in structure-based virtual screening. *Phys Chem Chem Phys*. 2020; 22(6): 3149–3159. <https://doi.org/10.1039/C9CP06303J>
- [16] Kamchonwongpaisan S, Charoensetakul N, Srisuwannaket C, Taweechai S, Rattanajak R, Vanichtanankul J, Vitsupakorn D, Arwon U, Thongpanchang C, Tarnchompoo B, Vilaivan T, Yuthavong Y. Flexible diaminodihydrotriazine inhibitors of *Plasmodium falciparum* dihydrofolate reductase: Binding strengths, modes of binding and their antimalarial activities. *Eur J Med Chem*. 2020;195: 112263. <https://doi.org/10.1016/J.EJMECH.2020.112263>
- [17] Somandi K, Seanego TD, Dlamini T, Maree M, de Koning CB, Vanichtanankul J, Rattanajak R, Saeyang T, Yuthavong Y, Kamchonwongpaisan S, Rousseau AL. Molecular docking studies, synthesis and biological evaluation of substituted pyrimidine-2,4-diamines as inhibitors of *Plasmodium falciparum* dihydrofolate reductase. *ChemMedChem*. 2022; 17(22): e202200418. <https://doi.org/10.1002/CMDC.202200418>
- [18] Opo FADM, Rahman MM, Ahammad F, Ahmed I, Bhuiyan MA, Asiri AM. Structure based pharmacophore modeling, virtual screening, molecular docking and ADMET approaches for identification of natural anti-cancer agents targeting XIAP protein. *Sci Rep*. 2021; 18(11): 4049. <https://doi.org/10.1038/s41598-021-83626-x>
- [19] Kyei LK, Gasu EN, Ampomah GB, Mensah JO, Borquaye LS. An in silico study of the interactions of alkaloids from *Cryptolepis sanguinolenta* with *Plasmodium falciparum* dihydrofolate reductase and dihydroorotate dehydrogenase. *J Chem*. 2022; 2022: 1–26. <https://doi.org/10.1155/2022/5314179>
- [20] Durán-Iturbide NA, Díaz-Eufracio BI, Medina-Franco JL. In silico ADME/Tox profiling of natural products: A focus on BIOFACQUIM. *ACS Omega*. 2020; 5(26): 16076–1684. <https://doi.org/10.1021/acsomega.0c01581>
- [21] Azzam KM Al. SwissADME and pkCSM Webservers Predictors: an integrated online platform for accurate and comprehensive predictions for in silico ADMET properties of artemisinin and its derivatives. *Complex Use Miner Resour*. 2023; 325(2): 14–21. <https://doi.org/10.31643/2023/6445.13>
- [22] Pires DEV, Blundell TL, Ascher DB. pkCSM: Predicting small-molecule pharmacokinetic and toxicity properties using Graph-Based Signatures. *J Med Chem*. 2015; 58(9): 4066–4072. <https://pubs.acs.org/doi/10.1021/acs.jmedchem.5b00104>
- [23] Purwanto BT, Hardjono S, Widiandani T, Nasyanka AL, Siswanto I. In silico study and ADMET prediction of N-(4-fluorophenylcarbamoithiyl)benzamide derivatives as cytotoxic agents. *J Hunan Univ Sci*. 2021; 48(2): 78–85.
- [24] Yeni Y, Rachmania RA. The prediction of pharmacokinetic properties of compounds in *Hemigraphis alternata* (Burm.F.) T. Ander leaves using pkCSM. *Indones J Chem*. 2022; (4): 1081–1089. <https://doi.org/10.22146/ijc.73117>
- [25] Walters WP. Going further than Lipinski's Rule in drug design. *Expert Opin Drug Discov*. 2012; 7(2): 99–107. <https://doi.org/10.1517/17460441.2012.648612>
- [26] Jia CY, Li JY, Hao GF, Yang GF. A drug-likeness toolbox facilitates ADMET study in drug discovery. *Drug Discov Today*. 2020; 25(1): 248–258. <https://doi.org/10.1016/j.drudis.2019.10.014>
- [27] Taidi L, Maurady A, Britel MR. Molecular docking study and molecular dynamic simulation of human cyclooxygenase-2 (COX-2) with selected eutypoids. *J Biomol Struct Dyn*. 2022; 40(3): 1189–1204.

- <https://doi.org/10.1080/07391102.2020.1823884>
- [28] Mosquera-Yuqui F, Lopez-Guerra N, Moncayo-Palacio EA. Targeting the 3CLpro and RdRp of SARS-CoV-2 with phytochemicals from medicinal plants of The Andean Region: Molecular docking and molecular dynamics simulations. *J Biomol Struct Dyn*. 2022; 40(5): 2010–2023. <https://doi.org/10.1080/07391102.2020.1835716>
- [29] Menéndez CA, Accordino SR, Gerbino DC, Appignanesi GA. Hydrogen bond dynamic propensity studies for protein binding and drug design. *PLoS One*. 2016;11(10):e0165767. <https://doi.org/10.1371/journal.pone.0165767>
- [30] El-Shamy NT, Alkoud AM, Hussein RK, Ibrahim MA, Alhamzani AG, Abou-Krissha MM. DFT, ADMET and molecular docking investigations for the antimicrobial activity of 6,6'-Diamino-1,1',3,3'-tetramethyl-5,5'-(4-chlorobenzylidene)bis[pyrimidine-2,4(1H,3H)-dione]. *Molecules*. 2022; 27(3): 620. <https://doi.org/10.3390/molecules27030620>
- [31] Tsuneda T, Song JW, Suzuki S, Hirao K. On Koopmans' Theorem in Density Functional Theory. *J Chem Phys*. 2010;133(17):174101. <https://doi.org/10.1063/1.3491272>
- [32] Giordano D, Biancanello C, Argenio MA, Facchiano A. Drug design by pharmacophore and virtual screening approach. *Pharmaceuticals (Basel)*. 2022;15(5):646. <https://doi.org/10.3390/ph15050646>
- [33] Imrie F, Bradley AR, Deane CM. Generating property-matched decoy molecules using deep learning. *Bioinformatics*. 2021; 37(15): 2134–2141. <https://dx.doi.org/10.1093/bioinformatics/btab080>
- [34] Heinzke AL, Zdrzil B, Leeson PD, Young RJ, Pahl A, Waldmann H, Leach AR. A compound-target pairs dataset: differences between drugs, clinical candidates and other bioactive compounds. *Sci Data*. 2024;11(1):1160. <https://doi.org/10.1038/s41597-024-03582-9>
- [35] Naz S, Farooq U, Khan S, Sarwar R, Mabkhot YN, Saeed M, Alsayari A, Muhsinah AB, Ul-Haq Z. Pharmacophore model-based virtual screening, docking, biological evaluation and molecular dynamics simulations for inhibitors discovery against α -tryptophan synthase from *Mycobacterium tuberculosis*. *J Biomol Struct Dyn*. 2021;39(2):610-620. <https://doi.org/10.1080/07391102.2020.1715259>
- [36] Torres PHM, Sodero ACR, Jofily P, Silva-Jr FP. Key topics in molecular docking for drug design. *Int J Mol Sci*. 2019;20(18):4574. <https://doi.org/10.3390/IJMS20184574>
- [37] Van Der Spoel D, Lindahl E, Hess B, Groenhof G, Mark AE, Berendsen HJC. GROMACS: Fast, Flexible, and free. *J Comput Chem*. 2005; 26(16): 1701–1718. <https://doi.org/10.3390/IJMS20184574>
- [38] Zoete V, Cuendet MA, Grosdidier A, Michielin O. SwissParam: A Fast Force Field Generation Tool for Small Organic Molecules. *J Comput Chem*. 2011; 32(11): 2359–2368. <https://doi.org/10.1002/JCC.21816>
- [39] Vanommeslaeghe K, Hatcher E, Acharya C, Kundu S, Zhong S, Shim J, Darian E, Guvench O, Lopes P, Vorobyov I, Mackerell AD. CHARMM general force field: A Force field for drug-like molecules compatible with The CHARMM All-atom additive biological force fields. *J Comput Chem*. 2010; 31(4): 671–690. <https://doi.org/10.1002/JCC.21367>
- [40] Boonstra S, Onck PR, Van Der Giessen E. CHARMM TIP3P Water model suppresses peptide folding by solvating the unfolded state. *J Phys Chem B*. 2016; 120(15): 3692–3698. <https://doi.org/10.1021/acs.jpcc.6b01316>
- [41] Luo J, Xue ZQ, Liu WM, Wu JL, Yang ZQ. Koopmans' Theorem for large molecular systems within density functional theory. *J Phys Chem A*. 2006; 110(43): 12005–12009. <https://doi.org/10.1021/JP063669M>